# SLAC – INFN Summer Exchange Program 2016

*Carlo Gilardi*

## SuperCDMS Experiment: study on muon background and on coaxial cable mechanical tension

## 1. Introduction

The SuperCDMS Snolab is one of the several experiments whose goal is to directly detect WIMPs, which means Weakly Interacting Massive Particles and represent one of the main candidates of the Dark Matter. In particular, the detectors are based on cylinders of Germanium or Silicon kept at Cryogenic temperature: an incoming WIMP can scatter with the nuclei of the semiconductor, produce primary phonons and electron-hole pairs. In the HV (High Voltage) detectors, the pairs are accelerated by the voltage imposed at the two basis of the detector and produce secondary phonons via the Neganov-Luke effect. Part of this phonons will reach the base of the detectors and will break some cooper pairs in a fin of superconducting Aluminum. The quasi particles produced in this way will travel inside the fin till they reach the interface between aluminum and the TES (Transition Edge Sensor), which is made by Tungsten. Since the superconducting gap in tungsten is lower than in aluminum, the quasi particles that pass from the latter to the former will lose energy, heating up the TES. Since the TES is kept at a temperature close to the critical temperature for the superconductive transition, the increase in temperature will cause an increase in the resistivity of the TES. Thus, since the TES is biased with a constant voltage, the current flowing in it will change. Eventually, the TES is coupled with a SQUID, sensitive to small change in current and able to give the output signal related to the WIMP interaction.

During my experience, I have worked on two different topics:

- The detectors are fabricated and tested in laboratories at the surface or at shallow depths underground. Hence, the muons' background cannot be ignored, since the walls and floors of the building are not able to stop them completely. Thus, it is necessary to estimate the rate at which the muons will hit the detector and the effects this will cause in the output signal. For this reason, I have studied this background and the current induced in the detector, as a function of depth.

- The detector is placed in a cryogenic fridge at around 30 mK. In order to read out the signal, this stage is connected to other stages at different temperature. Part of these electronic connections is made with superconducting coaxial cables in NbTi. This wires are strained and fixed in a copper housing. This procedure is done at room temperature and since the thermal contraction is bigger for copper than what it is for NbTi, it is necessary to prove that there is still enough mechanical tension in the wire even at cryogenic temperature. For this purpose, I have measured the tension of a coaxial cable at 77 K and verify there is a residual tension. Below 77 K, the contraction is negligible, hence it is not necessary to go to lower temperatures.

# 2. Summary

# 3. Muon Background study

## 3.1 Surface Spectrum

In order to calculate the flux of muons that are able to reach a detector at a certain depth underground, it is firstly necessary to find a good model that describes the muons spectrum at the surface, at the sea level. In fact, the more common models employed when calculating the muons background are able to describe only the upper part of the spectrum, above 100 GeV. In fact, the low part of the spectrum in useless to describe the background in experiments that are conducted some kilometers underground, since the majority of low energy muons are stopped. On the contrary, for laboratories that are in a building on the surface or anyway only some meters underground, the most important part of the spectrum is the low part, from 0.1 GeV to 10 GeV. Hence, it is necessary to find a good model that describes both the lower part and the higher part of the spectrum. The starting point is the Gaisser formula (Gaisser – 1990):

$$\Phi(E,\theta) = AE^{-\gamma}\left(\frac{1}{1 + E'cos\theta/E_\pi} + \frac{B}{1 + E'cos\theta/E_\kappa} + r\right)$$

In the formula we can notice three terms in the parenthesis: the first is related to the muons that come from the decay of pions, the second term is related to the decay of kaons, while the third term is related to the prompt muons, already present in the cosmic rays. The parameters present in the formula are adjusted to reproduce the experimental results in the various range on energy.

Before introducing the various parameters, it is necessary to make some consideration about the angle. In fact, the angle $\vartheta$ that appears in the formula is the zenith angle and its cosine is related to the path travelled by the muons in the atmosphere. However, for high zenith angle, it is necessary to take into account the fact that the Earth is not flat, hence the effective path travelled in the atmosphere will be lower than the one calculated using $cos\vartheta$. For this reason, we can introduce an effective angle that is able to reproduce this effect, as done by Lesparre (2010):

$$cos\theta^* = \sqrt{1 - \frac{1 - cos^2\theta}{(1 + H/R)^2}}$$

Where H is the altitude of production of muons (32 km) and R is the Earth's radius (6370 km).

Following the work of Tang (2006), it is possible to identify three different range of energy, in order to describe the spectrum:

- High Energy: above 100/$cos\vartheta^*$ GeV. In this region the original Gaisser parametrization is used: E'=E, A=0.14, B=0.054, γ=2.7, $E_\pi$=115/1.1, $E_k$=850/1.1 and r=0
- Middle Energy: from 1/ $cos\vartheta^*$ GeV to 100/$cos\vartheta^*$ GeV. In this region we consider: E'=E-Δ, r=$10^{-4}$ and:

$$A = 1.1 * 0.14 * \frac{90\sqrt{cos\theta + 0.001}}{1030}^{\frac{1.3}{Ecos\theta^*}}$$

and where:

$$\Delta = 2.06 * 10^{-3}\left(\frac{950}{cos\theta^*} - 90\right)$$

- Low Energy: below 1/ $cos\vartheta^*$ GeV. Here it is sufficient to make the following substitution:

$$E = \frac{3E + 7/cos\theta^*}{10}$$

With this model, the spectrum is the one in figure 1. As it can be seen, the spectrum increases up 1 GeV and then starts decreasing with the typical exponential behavior with exponent 2.7.
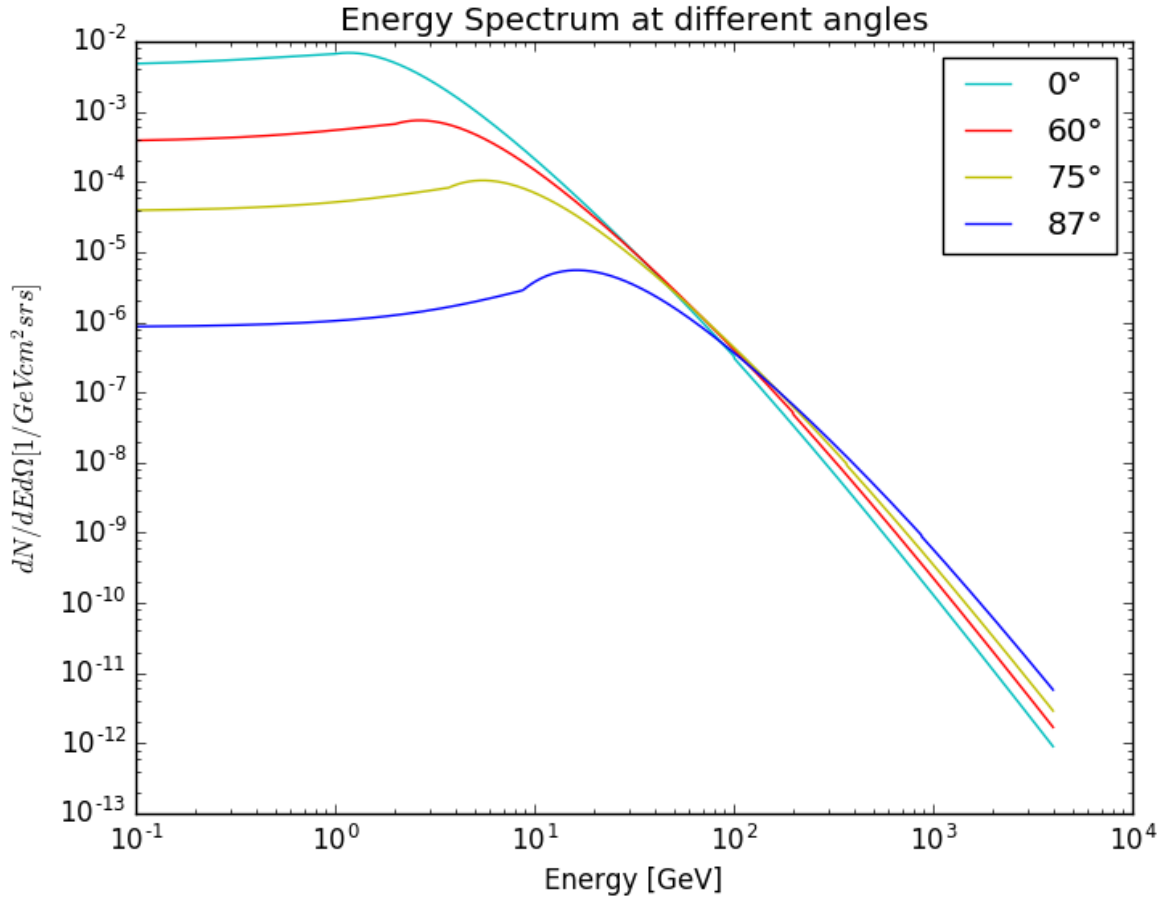


Figure 1: Energy spectrum for muons. Four different zenith angles are plotted: 0°, 60°, 75° and 87°. At low energies, the majority of the muons are vertical, while at higher energies the muons are more horizontal.

We can also plot the angular dependence of the spectrum (figure 2). Here it can be noticed the different behavior of the different ranges of energy. In fact, low energy muons (up to 10 GeV) are mostly vertical. On the contrary, as the energy increases, the spectrum becomes firstly isotropic (100 GeV) and then horizontal (1000 GeV). The spectrum is built fitting the experimental data, but we can still explain this phenomenon: indeed, high energy muons are produced by the decay of high energy pions. These particles are very fast and if they come vertically, the atmosphere is not enough deep for them to decay. On the contrary, if they have a high zenith angle, the high energy pions have time and space to decay and produce high energy muons. Hence, the model is able to describe this effect. Eventually, this fact is not so important, since, as we can see in figure 1, the number of muons at 1000 GeV is way lower than the muons below 10 GeV. As a conclusion, we can say that the flux of muons is mainly vertical. This is clearly due to the fact that high zenith angle muons must travel more and they are more likely to decay.

With the same spectrum I have also calculated the directional intensity: this values correspond to the integral of the spectrum over energy, along a certain direction. For example, an important value used to describe the spectrum at different depths is the vertical muon intensity, which is, according to this model:
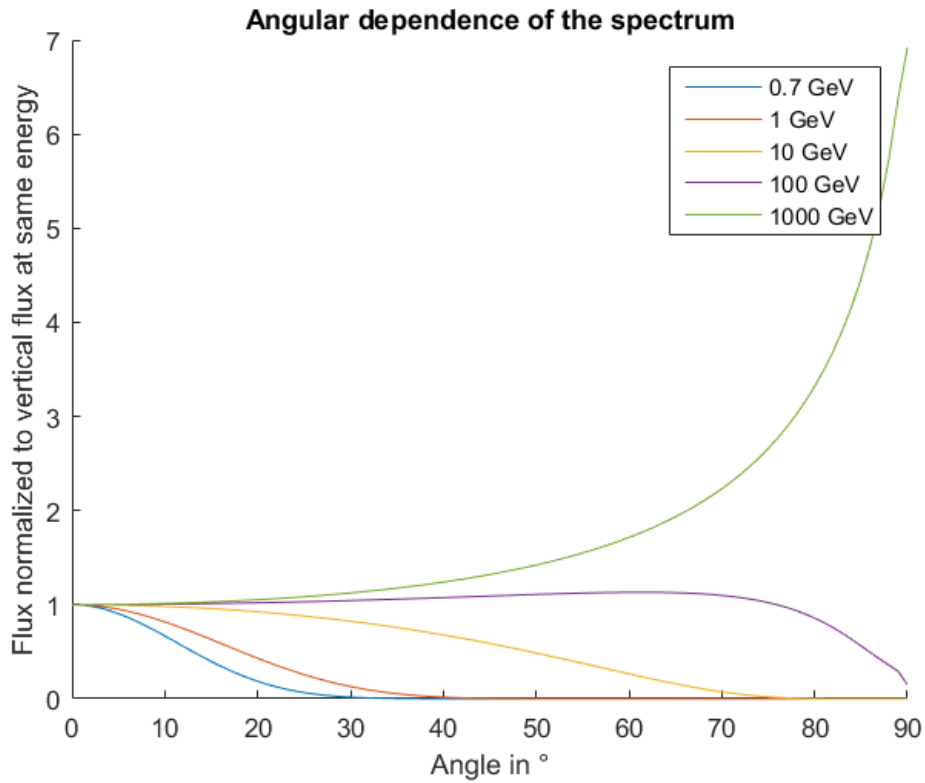
$$I^v = 0.0228 \frac{1}{cm^2 srs}$$

4

*Figure 2: Angular dependence of the muons' spectrum at different energies. We can see the behavior at different ranges of energy: low energy vertical, middle energy isotropic and high energy horizontal.*

In figure 3 there is also the directional intensity as a function of the zenith angle: the typical $\cos\vartheta^2$ behavior can be recognized. Another parameter that can be calculated is the total flux, which is the integral over energy and angle. At the surface, we obtain a flux equal to:

$$F = 0.0468 \frac{1}{cm^2 s}$$

Especially at low energies, the spectrum is influenced by some non-constant factors. In fact, the cosmic ray flux depends on the solar modulation, on the latitude of the location of the experiment, on the pressure and temperature of the atmosphere, on the altitude and on many variable parameters. In particular, the solar cycle of 11 years modulates the low part of the spectrum, causing a change of 5-10 % in the spectrum up to 10 GeV. The latitude, moreover, affects the spectrum up to 5 GeV since the magnetic field of the Earth tends to deviate low energy particles. The consequence is a difference in the low part of the spectrum between experiments held at the equator and experiments held near the pole for example. For all these reasons, it is difficult to find a model that well describes the data on the low part of the spectrum, since often the data are not in agreement with each other. Anyway, I have considered this small modification negligible, since the cause a variation lower than 20% and hence they do not affect too much the rate of muons that are able to hit the detectors.
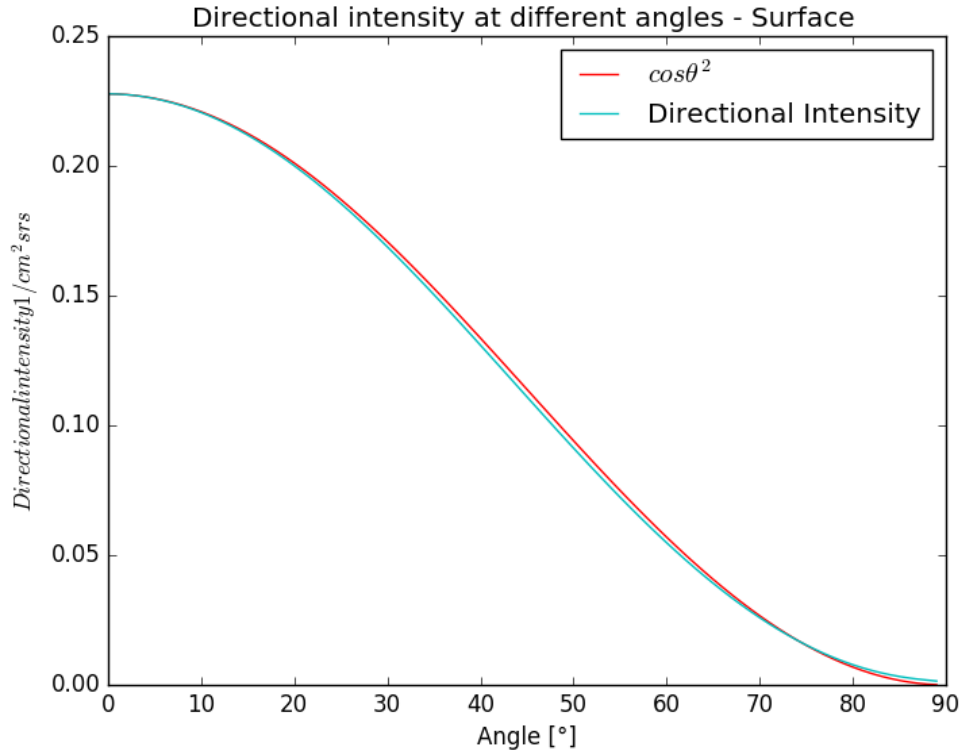
*Figure 3: Angular dependence of the muons' spectrum. It can be seen the behavior at different ranges of energy: low energy vertical, middle energy isotropic, high energy horizontal. The values of the spectrum are normalized to the vertical value for each energy.*

## 3.2      Spectrum at Shallow Depths

As a muon reaches the surface, it will start penetrating inside the ground and will lose energy, according to the stopping power related to the material that compose the ground. Eventually, after crossing a certain depth of ground, it will reach the detector. Anyway, the probability of decay will increase, since there is a finite time between the moment the muon arrives at the surface and the instant in which it hits the detector. The model I propose to describe how the spectrum change going underground, takes into account these two effects: the loss of energy and the increasing decaying probability. I did not take into account the generation of secondary particles (as neutrons) and the scattering of the muons. In fact, these two are secondary order corrections and I was able to obtain good enough results with the simpler model.

The general formula for the stopping power is the following:

$$-\frac{dE}{d\varrho} = a(E) + b(E)E$$

Where a(E) is related to the energy loss caused by ionization of the atoms present in the material, b(E) is related to the radiative energy loss and ϱ is the opacity and it is defined as:

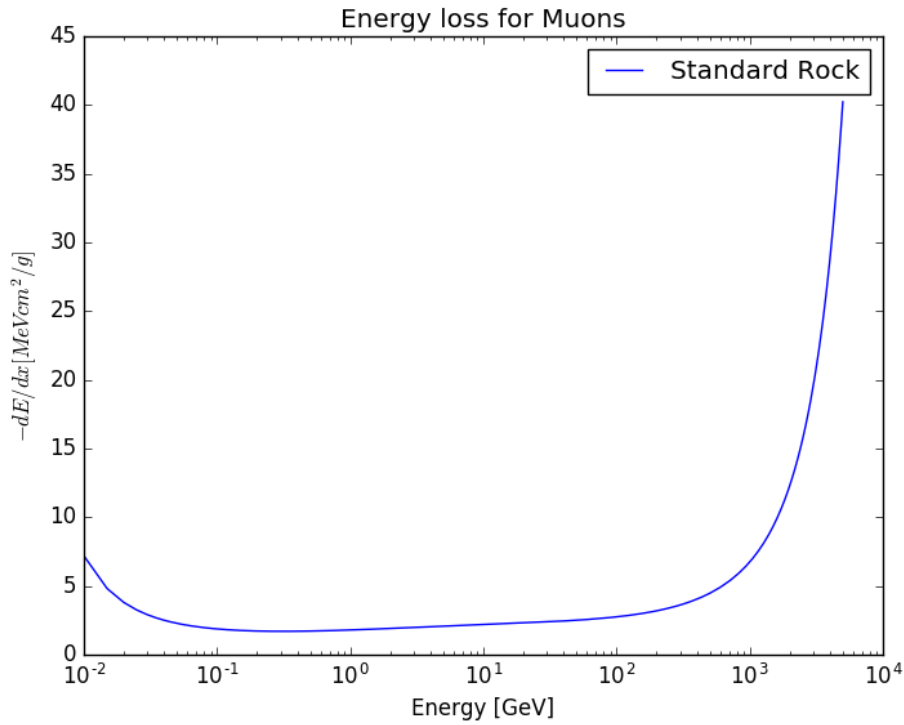$$\varrho(L) = \int_{L} \rho(\xi)d\xi$$

6

*Figure 4: Fit of the stopping power for standard rock. We can recognize three regions: a sub-relativistic regime, up to 0.5 GeV, a minimum ionizing regime, up to 100 GeV, with a constant stopping power, and a high energy regime, with high radiative losses.*

In the case of a single material with constant density, we have just:

$$\varrho(L) = \rho * L$$

And we can see that the opacity is nothing but a weighted length. In fact, the stopping power depends mainly on the density of the material crossed. The a and b parameter have a behavior that is quite general, which means that each material has more or less the same trend. Anyway, for our purposes, I have considered a formula that fits the stopping power of muons travelling in standard rock. In fact, the density and the properties of the rock (2.65 g/cm$^3$) are similar to those of concrete (density 2.4 g/cm$^3$).
Hence, following the work of Lesparre (2010), I have used the following formula:

$$\frac{dE}{d\varrho} = -10^{l_4 y^4 + l_3 y^3 + l_2 y^2 + l_1 y^1 + l_0} \left[ \frac{MeV cm^2}{g} \right]$$

Where y is the logarithm of the energy, expressed in GeV, and $l_0$=0.2549, $l_1$=0.0801, $l_2$=0.0368, $l_3$=-0.0461, $l_4$=0.0154.

Thus, as the muons are travelling inside matter, they will lose energy and hence they will slow down. If we consider that the energy is lost continuously (and not with discrete scatter events as it should be), we can calculate at every instant the velocity of a muon with a certain energy, and in this way calculate the period of time that spent by the muon to reach a certain depth, in its reference systems. At each depth, we can find the probability of decay of a muon with a certain energy and zenith angle and in this way modify the spectrum

according to this. I have made this for different depths: in figure 5 it is possible to observe how the spectrum varies at different depths and at different angles.
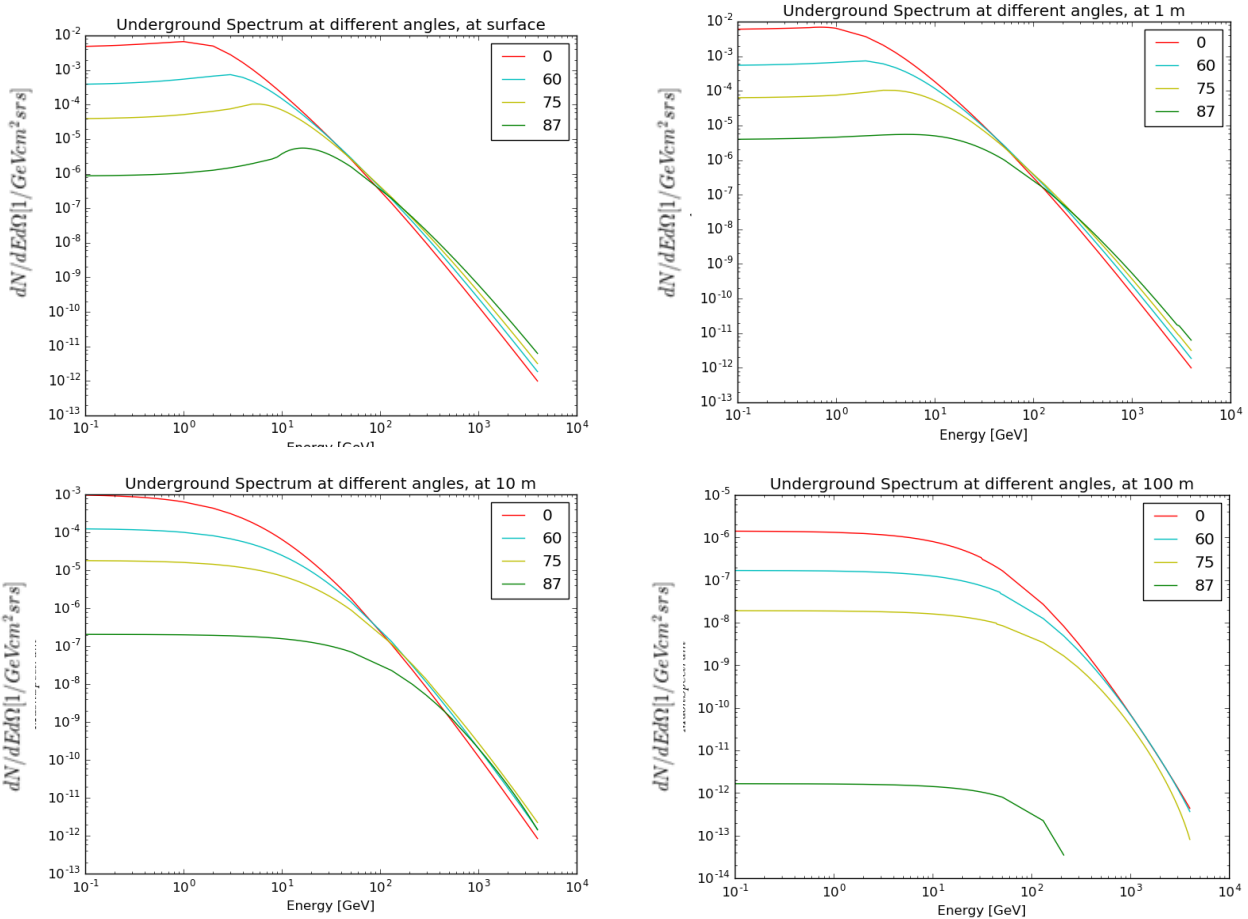


*Figure 5: Muon spectrum at different depths (surface, 1 m, 10 m and 100 m of standard rock) and different zenith angles (0°, 60°, 75° and 87°)*

The spectrum at 1 m is very similar to the one at the surface, even if we can still identify two effects, which are more evident at 10 and 100 m: the overall spectrum tends to decrease, since the muons are decaying and their total number decreases. Moreover, there is a shift towards lower energies, since all the muons are depositing some energy during their path. The overall spectrum is thus moving to the lower left angle. As the
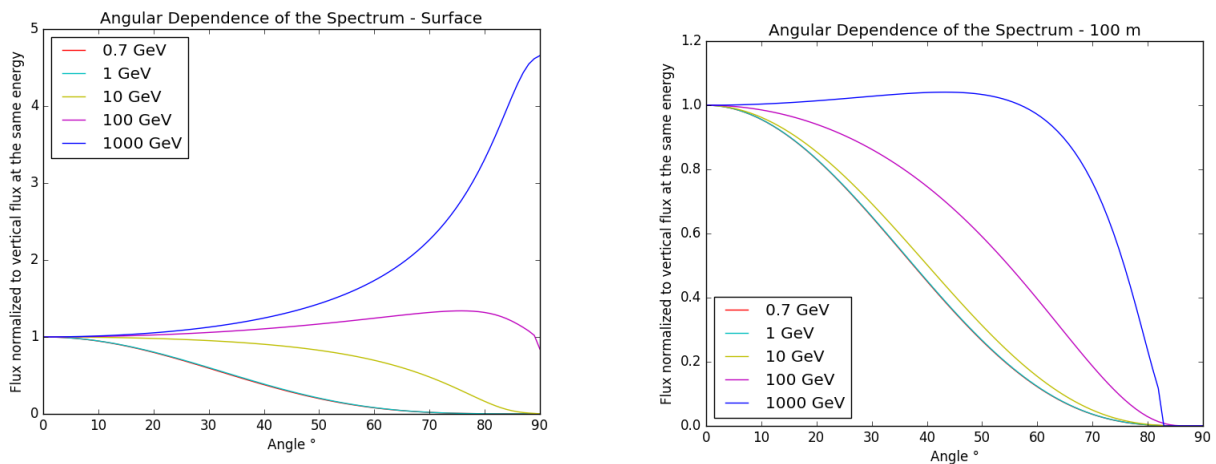


*Figure 6: Angular dependence of the spectrum at the surface and at 100 m of standard rock. At high depths, even high energy muons are no more horizontal.*

8

depth increases, finally, the part of the spectrum that is decreasing more rapidly is related to the high zenith angle muons, since their effective distance is 1/cosϑ greater with respect to the vertical muons.

This fact is evident also in figure 6, where I have plotted the angular dependence of the spectrum at the surface and at 100 m. In fact, at big depths, also the high energy muons start to become more vertical.
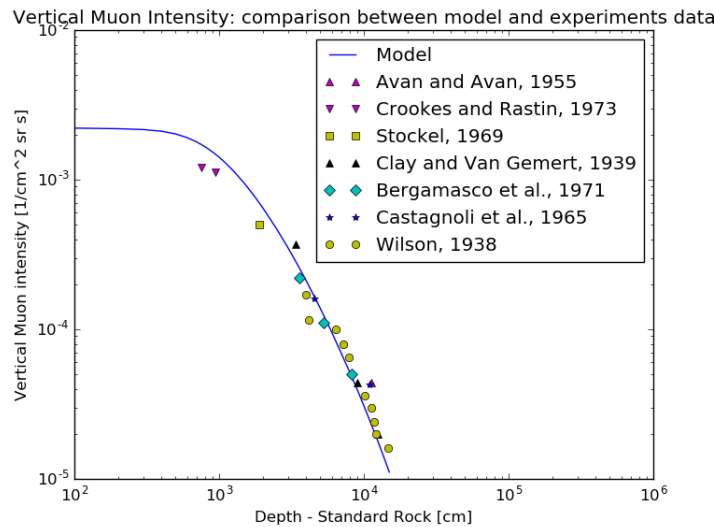


*Figure 5: Comparison between the vertical intensity obtained with the model (blue line) and some experimental data.*

A way to compare this model with experimental results is to calculate the vertical muon intensity at different depths. As it can be seen in figure 7, the model is in agreement with experimental data reported by Bugaev (2000). It is difficult to compare the model with data above 1 m of rock, since it is difficult to find data for this region, mainly because of it highly depends on non-constant variable, as latitude and the time of the measurement. At higher depths, the model is not adequate, since it does not take into account the generation of secondary muons and particles, which is the most important part at high depths. For our purposes they are anyway irrelevant.

Calculating the average energy and the average zenith angle of the flux of muons, we can observe that the average angle is constant around 26° (up to 25 m), while the energy, after a brief decreasing, increases and pass from 6 GeV at the surface to 13 GeV at 15 m of standard rock (figure 8). These values and the spectrum in general will be used in the next section to simulate the effect of a bunch of muons in the detector response.
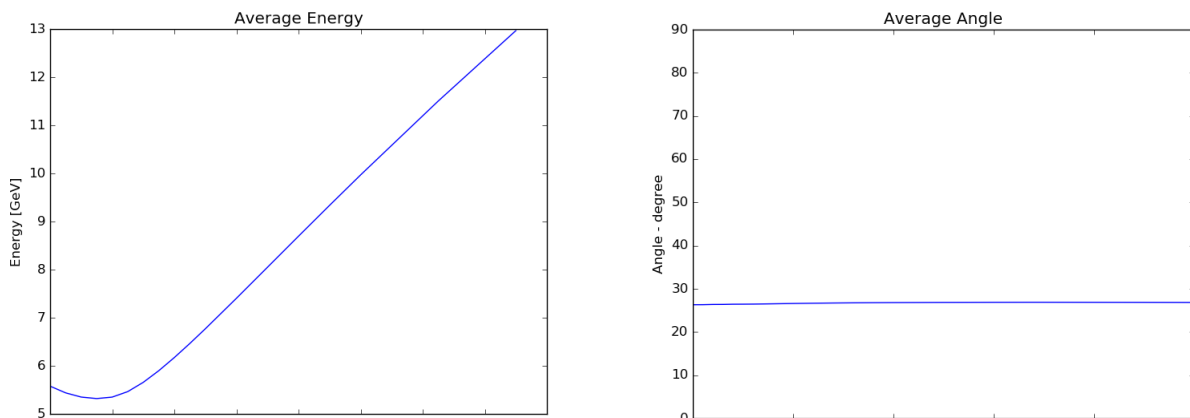


*Figure 6: Average energy and zenith angle as a function of depth. The angle is constant, while the average energy increases as the depth increases.*

The last thing to add is how to calculate the equivalent depth in standard rock centimeters. This is easily done with the following formula:

$$d_{mat} = d_{sr} \frac{\rho_{sr}}{\rho_{mat}}$$

Clearly, this takes into account only the difference in the density and not the difference in the a and b parameters. Anyway, the dependence of a and b on the material is not strong and can be neglected in first approximation. The table 1 shows some useful conversion with common material present in building or in shielding:

| Material | Water | Standard Rock | Concrete | Standard Rock | Lead | Standard Rock |
|---|---|---|---|---|---|---|
| Density | 1 | 2,65 | 2,4 | 2,65 | 11,34 | 2,65 |
| Depth [cm] | 0,50 | 0,19 | 0,50 | 0,45 | 0,50 | 2,14 |
| | 1,00 | 0,38 | 1,00 | 0,91 | 1,00 | 4,28 |
| | 2,00 | 0,75 | 2,00 | 1,81 | 2,00 | 8,56 |
| | 5,00 | 1,89 | 5,00 | 4,53 | 5,00 | 21,40 |
| | 10,00 | 3,77 | 10,00 | 9,06 | 10,00 | 42,79 |
| | 25,00 | 9,43 | 25,00 | 22,64 | 25,00 | 106,98 |
| | 50,00 | 18,87 | 50,00 | 45,28 | 50,00 | 213,96 |
| | 75,00 | 28,30 | 75,00 | 67,92 | 75,00 | 320,94 |

*Table 1: conversion table between standard rock and water, concrete and lead. Every couple of columns gives the correspondent depth in standard rock, given the depth in the actual material.*

### 3.3 Muon Induced Current

The first thing we can calculate with the spectrum is the rate of muons that are able to hit the detector. Since the detectors of the SuperCDMS experiments are cylindrical, I have considered only this shape and I have calculated the effective area projected to the place perpendicular to the direction of each muon, taking into account both the basis and the lateral area of the detector. I have considered three detectors:

- HV detector: diameter=10 cm, height=3.33 cm
- iZIP Soudan detector: diameter=7.62 cm, height=2.54 cm
- 10x10x4 detector: cubic detector with effective diameter=1.028 cm and effective height=0.354 cm

The last one is a cubic detector used for R&D. In order to use the same model for cylindrical detectors, I have considered effective basis and height in order to preserve the total area.

The total area seen at each angle is equal to:

$$A_{tot} = \frac{\pi}{4} d(d \, cos\vartheta + 2 \, h \, sin\vartheta)$$

To find the total rate of muons that hit the detectors, it is sufficient to integrate the spectrum over energy and angle and multiply each direction for the corresponding effective area. Moreover, it is also possible to consider sites that are for example on a hill. A very simple model consists in integrate the spectrum up to a certain angle, neglecting all the muons coming from the hill. Indeed, their fraction will be very small. In this way I have calculated the rate for the three detectors and compared them to the experimental data, which are a rate of one muon per minute for the 10x10x4 and a rate of 0.7 Hz for the iZIP detector on a hill of 30°.
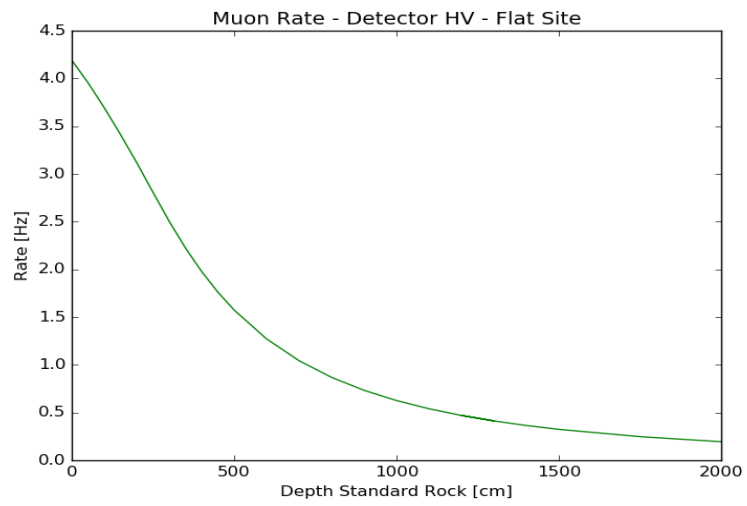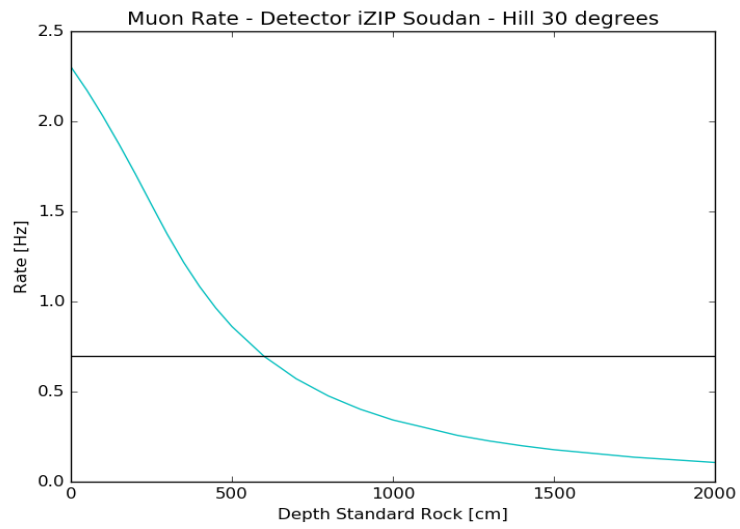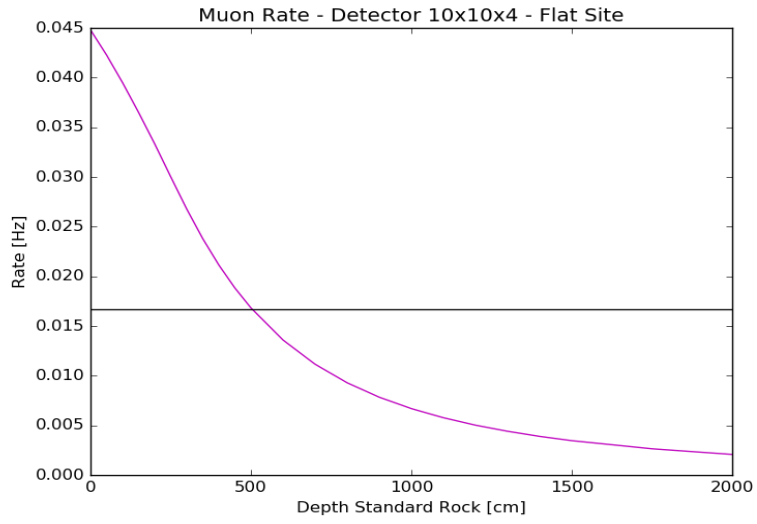
*Figure 7: Rate of muons in 10x10x4, iZIP Soudan and HV detectors. The black lines are the rate observed experimentally.*

The figure 9 shows the rates in the three detectors at different depths. In particular, we see that for the 10x10x4 detector, a rate of one muon per minute correspond to 5 m of standard rock. Considering that the experiment site is in the Underground Stanford Facility, the result is consistent with the building that are over it. Also for what concerns the iZIP detector, a rate of 0.7 Hz corresponds to 6 m of standard rock. The site is a basement and there is also a lead shielding of some centimeters. Again, the result is plausible.

In order to find the effect in the response of the detector caused by a muon, it is necessary to find firstly the energy deposited onto the detector by a muon with a certain energy and zenith angle, secondly the amount of pairs produced and the corresponding phonons flux and finally the change in the current flowing in the TES caused by this flux.

To estimate the deposited energy, I have employed the Bethe Bloch equation, which is just the stopping power that take into account only the ionization losses. In fact, in first approximation I have neglected the pairs created by the photons produced via radiative emission from the muons. With the Bethe Bloch equation is possible to find the energy lost by a muon of a certain energy that is travelling inside a germanium detector. This energy loss is plotted in figure 10.
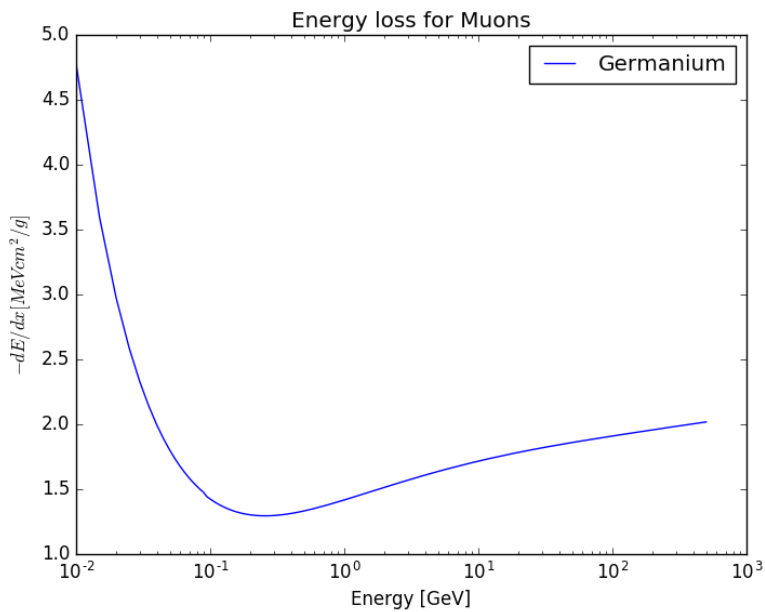


*Figure 8: Bethe Bloch equation for Germanium. The energy loss is high at energies below 0.1 GeV and almost constant above.*

The stopping power needs to be multiplied times the density of the Germanium and the path travelled by the muons. To calculate the path, I have considered an average that depends only on the zenith angle, the diameter and the height. In this way I have obtained the following formula:

$$path = \frac{2\,d\,h}{2\,d\,cos\vartheta + \pi\,h\,sin\vartheta}$$

Once obtained the energy deposited by each muon (depending on its energy and zenith angle), we can calculate the number of pairs produced. Since the Germanium is a semiconductor with indirect bandgap, we assume that the average energy necessary to create a pair is around 3 eV. In fact, when the muon deposits its energy, an electron will be excited to the conduction band and will scatter producing primary phonons in its way down to the L valley in the conduction band. The energy necessary for this process and for the primary phonons emission is indeed 3 eV. Later, the pairs will be accelerated by the electric field, they will reach a

drift velocity and all the work performed by the electric field will cause the emission of a flux of Luke-Neganov phonons. The energy associated to this flux can be obtained with the following formula:

$$E_{ph} = E_{dep}\left(\frac{V - \varepsilon_{bd}}{\varepsilon_{pair}} + 1\right)$$

Where $E_{dep}$ is the energy deposited by the muon, $\varepsilon_{bd}$ is the indirect bandgap in Germanium (0.66 eV) and $\varepsilon_{pair}$ is the 3 eV parameter discussed above. This formula gives the energy of both the primary and the Luke phonons.

As described in the introduction, when the phonons reach the surface, they break the cooper pairs inside the Al fins, producing quasi particles that diffuse in the TES, heating it up. When the temperature of the TES increases, its resistance increases too and the current decreases. This happens until the temperature is high enough such that the TES is away from the superconducting transition and the resistance is constant at its normal value. In this case, the current saturates at a certain value. Then, the TES starts cooling down, with a certain time constant, until the it reaches the critical temperature, where the resistance starts decreasing and the current increases. Eventually, the current comes back to its original working value.

In order to find the response of the detector, I have made some approximations. In particular I have considered that the flux of phonons hits the surface only in a small area. This is not true in general, since the area that will be hit by phonons depends on the position of the pair production. Moreover, I have considered the decay time equal to the ratio between heat capacitance and heat conductance. I did not take into account their dependence with temperature, for simplicity. In particular, the capacity of the TES is equal to:

$$C_{T_c} = f_{SC}\, c_W V_{TES,eff} T_c$$

Where $c_W$ is the specific heat capacity of tungsten, $f_{SC}$ is the correction to the normal value to take into account the capacity of cooper pair breaking in the superconducting transition, $T_c$ is the critical temperature and $V_{TES,eff}$ is the sum of the volume of the TES and of the connection between TES and Al fins.

The heat exchanged between the TES and the bath can be linearized around the critical temperature, in order to obtain the heat conductance between the TES and the bath, that can be written as:

$$G = n\Sigma V_{TES,eff} T_c^{n-1}$$

Where $\Sigma$ is the electron-phonon coupling constant and n is the exponent of the thermal conduction power law. With these parameters, the decay time constant results equal to:
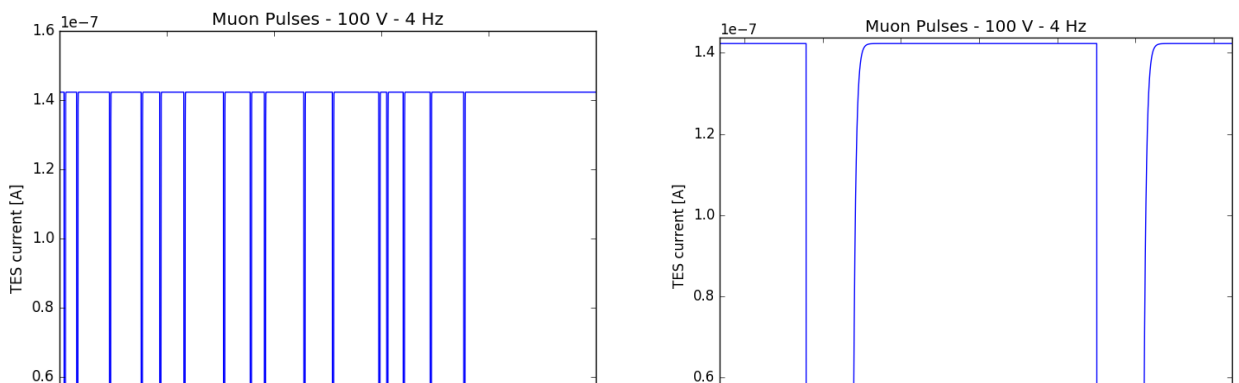
$$\tau = 592\ \mu s$$



*Figure 9: On the left: response in HV detector at the surface, with 100 V. The rate is around 4 Hz. On the right: two particular peaks in the current: the first correspond to a muon of 7.53 GeV and angle 13°; the second to a muon of 3.22 GeV and 21°. The energy of the phonons flux, coupled to a TES, are respectively 1.5 and 1.37 \*10-10 J*

13

With the spectrum obtain in the previous section, the parameters of each detector and the depth, it is possible to simulate the response of the detector. In figure 11 it is possible to see the simulation of the response of a HV detector at the surface. In figure 12 there is the comparison between the responses of the iZIP detector, with a voltage of 0 V and 100 V.
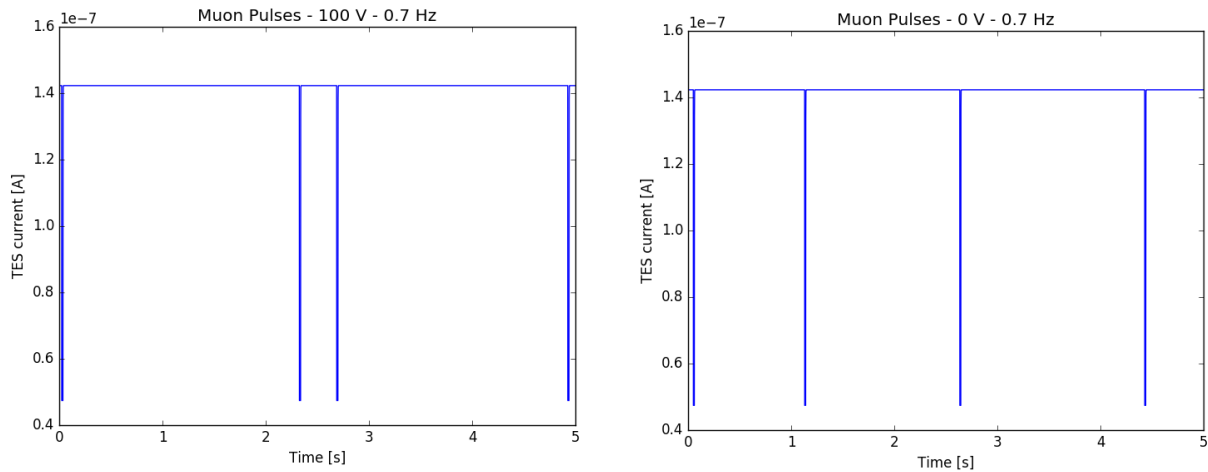


*Figure 10: Response for iZIP detector at 6 m underground, with a rate of 0.7 Hz. On the right: 0 V, the four peaks are relative to muons with energies 1.46 GeV, 2.97 GeV, 2.41 GeV, 8.10 GeV and angles 2°, 34°, 60°, 2°. The energy deposited by phonons are 2.45 \* $10^{-12}$ J, 2.37\* $10^{-12}$ J, 2.73 \* $10^{-12}$ J, 2.82\* $10^{-12}$ J. On the left: 100 V, the four peaks are relative to muons with energies 18.33 GeV, 1.06 GeV, 3.70 GeV, 5.37 GeV and angles 29°, 70°, 15°, 27°. The energy deposited by phonons are 1.17 \* $10^{-10}$ J, 1.27 \* $10^{-10}$ J, 1.07 \* $10^{-10}$ J, 1.08 \* $10^{-10}$ J.*

We can observe few things: firstly, considering one bias condition, the energy of the phonons flux is practically equal for every muon. In fact, the majority of the muons are minimum ionizing particles and the energy they deposit is always the same. Moreover, the dependence on the angle is not so strong, due to the shape of the detectors. Comparing the two different bias condition, however, we can notice that the energy of the phonons changes by two order of magnitude. Since the current saturates, the only consequence is to have thicker peaks, that decay in time with the same time constant.

### 3.4 Conclusions

The study of the spectrum of muons at different depths predicts results that are in agreement with the experimental values. Knowing the spectrum, moreover, it is now possible to simulate the flux of muons that hit a detector of arbitrary size at an arbitrary depth with different shielding materials. In this way, the response of the TES can be obtained. The following step is to calculate the power spectral density of the signal of the muons, considered as a noise. To refine the model in order to get results more precise, it is necessary to study the exact influence of all the variables (solar modulation, location…) on the spectrum, in order to obtain a better parametrization for the muon flux at the place where the experiments are held. The description of secondary effects shouldn't be so important; hence it can be neglected. A better description of the heat generation and conduction is however necessary, since there are some effects which could affect the results. In particular, it is necessary to describe better the generation and propagation of the phonons and their coupling with the aluminum fins. Indeed, it is possible that part of the phonons is not absorbed, since their energy is lower than the superconducting gap in the aluminum. Therefore, they will heat up the detector, changing the time constant (since the capacitance and the conductance change).

14

# 4. Coaxial cable tension measurement

## 4.1 Experimental Setup

The coaxial cable is made of 4 NbTi wires, fixed in a copper housing with a tension of 40 g. Each wire is composed of NbTi coated with Cu. The total length is 26.6 cm and the coating has been etched off, leaving some copper only at the two ends, in order to be able to solder the wires to the board. These two un-etched parts are 2,66 cm long. The diameter of the NbTi is 31 μm, while the two ends have a diameter of 50 μm. The resistance of each wire is 180 Ω.

Neglecting the two un-etched parts and considering the system as a single wire with a certain linear density of mass μ, length and diameter, it is possible to find the relation between the tension and the resonance frequency:

$$f = \frac{1}{2L}\sqrt{\frac{T}{\mu}}$$

In order to measure the resonance frequency, it is possible to place the wire in a magnetic field, apply a sinusoidal current to the wire and measure the voltage across it. The magnetic field will act with a force on the wire, since there is a current flowing in it. Anyway, the oscillation of the wire is small if the frequency of the current is away from the resonance frequency of the wire, since it is highly damped. Once hit the resonance, however, the wire will start oscillating. In this condition, the electrons flowing in the in the wire will acquire a velocity which has a component perpendicular to the wire different from zero. Thus, they will experience a Lorentz force with a direction parallel to the wire, whose result will be to generate a EMF at the end of the wire. As a consequence, the voltage across it will change.
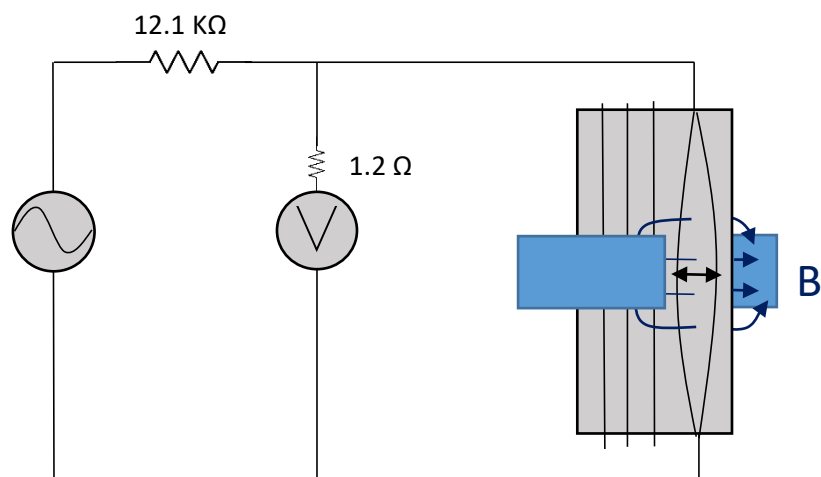


*Figure 13: Experimental setup: the 12.1 kOhm resistance in used to have a sinusoidal current generator. The voltmeter used to measure the voltage across the wire has an internal resistance of 1.2 Ohms.*

Firstly, I have measured the resonance frequency at room temperature, to verify the value of 40 g. Then, I have measured the frequency and the resistance of the wire going from room temperature to 77 K.

## 4.2 Room Temperature Measurement

In order to find the resonance frequency of the wire, I have swept the frequency from 100 Hz to 2500 Hz, with a step of 0.1 Hz. I have chosen a sinusoidal signal with a peak to peak voltage of 2 V: in this way the current flowing in the wire was around 80 µA, low enough not to ruin or heat the wire. The resolution of the voltmeter was 0.1 mV and the internal resistance 1.2 Ω. With this setup I was able to see the resonance peaks in each wire, as it can be seen in figure 14.
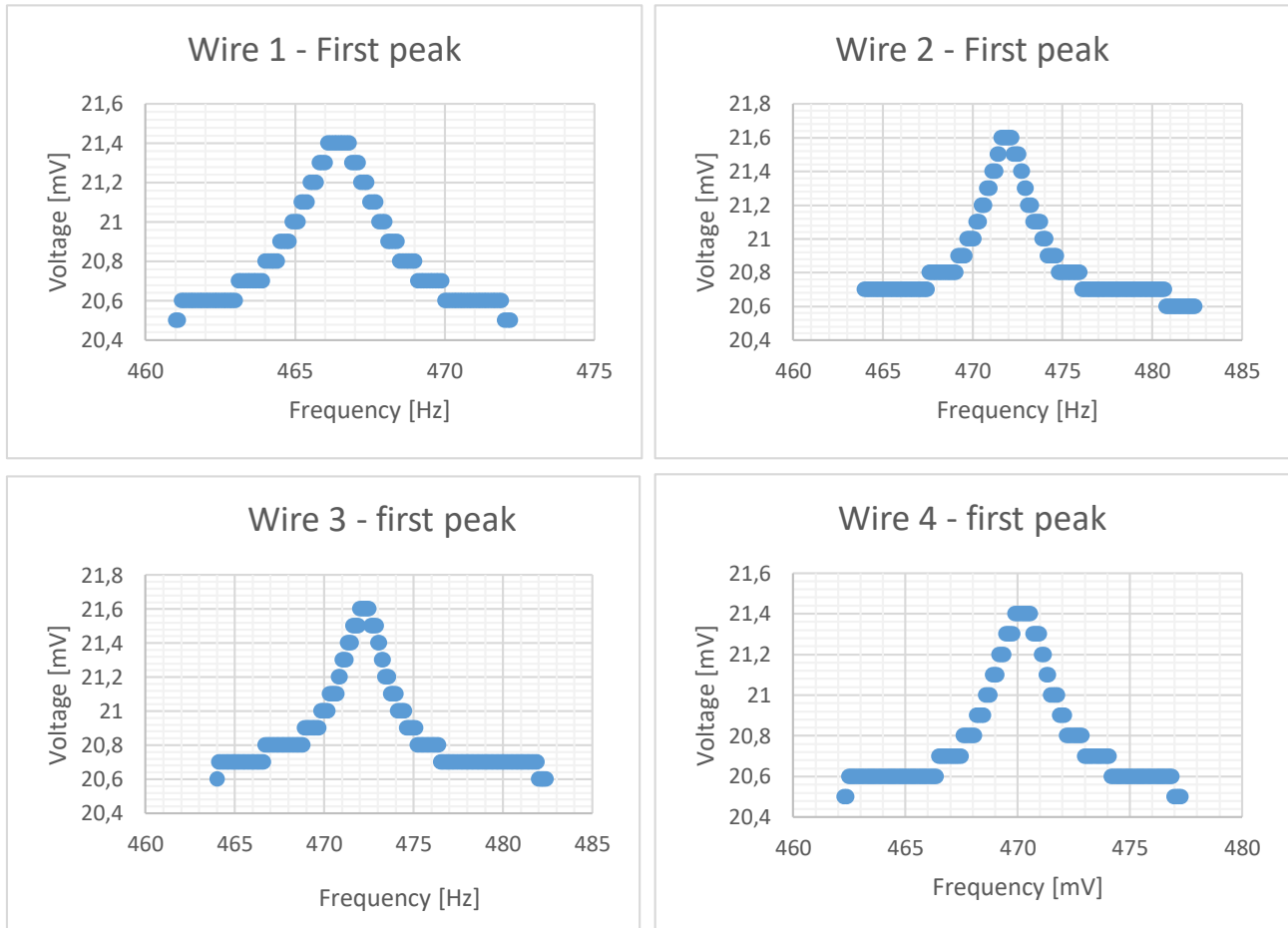


*Figure 14: resonance peaks for the 4 wires. All the peaks are clearly visible and are in agreement with each other, with a value around 470 Hz.*

As it can be seen, the peaks are symmetric and indicate that the resonance frequency is around 470 Hz. The frequencies are reported in table 1, together with the height and the width of the peak and the ratio between the voltage at the peak and the voltage away from resonance.

|        | Resonance Frequency [Hz] | Peak's Height [mV] | Peak's ratio | FWHM [Hz] |
|--------|--------------------------|--------------------|--------------|-----------|
| Wire 1 | 466.5                    | 0.9                | 0.044        | 3         |
| Wire 2 | 471.9                    | 1.0                | 0.049        | 3.6       |
| Wire 3 | 472.2                    | 1.0                | 0.049        | 3.7       |
| Wire 4 | 470.2                    | 0.9                | 0.044        | 4.8       |

*Table 2: Resonance peak, its height and width for the four wires.*

Only for the Wire 1, I have also tried to find higher harmonics. Since the magnet is in the middle, the even harmonics are suppressed, since the magnetic field force the wire not to have a node in the middle. Moving the magnet towards one end, it is possible to observe even the even harmonics.
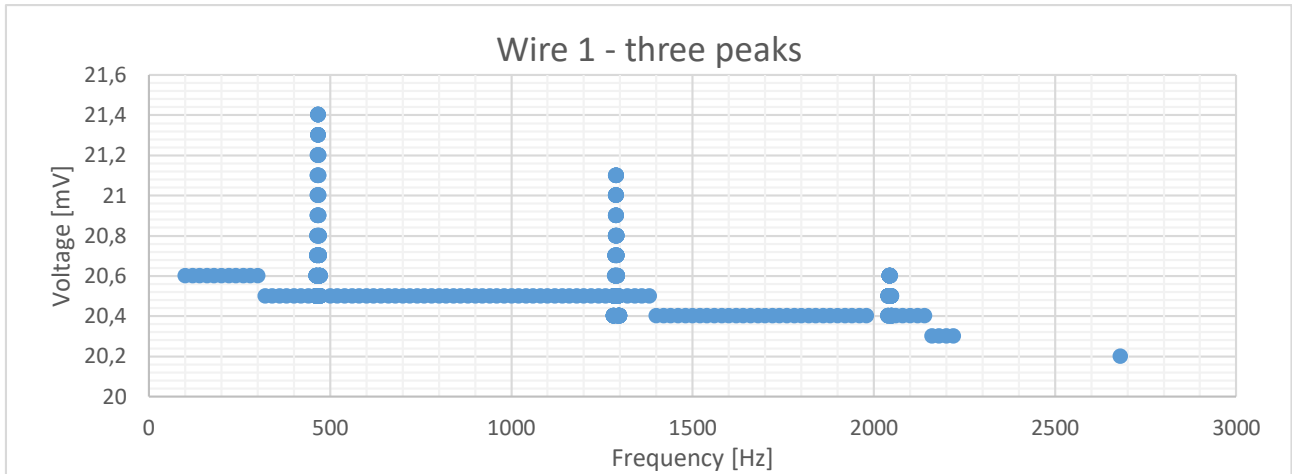
*Figure 15: resonance frequency and higher harmonics (third and fifth) for the first wire. The decreasing of the voltage at higher frequency can be due to capacitance effects.*

As it can be seen from figure 15, the three peaks are clearly visible. We can observe that the voltage across the wire decreases as the frequency increases: this can be due to a capacitance or an inductance in the circuit that decreases the impedance of the wire at higher frequency. Moreover, there is a shift in the frequencies of higher harmonics. In fact, being the normal mode at 466.5 Hz, the third and fifth peaks should be at 1399.5 Hz and 2332.5 Hz, while they are actually at 1288.6 Hz and 2043.7 Hz. This shift is greater at higher frequency and it indicates the possibility that even the first peak is shifted downwards. This would underestimate the tension and hence it does not represent a problem.

Neglecting this shift, we can calculate the tension of the wire, using the length and the diameter of the wire, the linear density (obtained averaging the density of Nb and Ti, since the wire is approximately 50% Nb and 50% Ti) and the frequency. We obtain the results in table 2.

|  | Wire 1 | Wire 2 | Wire 3 | Wire 4 |
|---|---|---|---|---|
| Frequency [Hz] | 466.5 | 471.9 | 472.2 | 470.2 |
| Tension [g] | 29.82 | 30.51 | 30.55 | 30.29 |

*Table 3: resonance frequency and tension for each of the four wires.*

The results are not totally in agreement with the theoretical value of 40 g. This can be due to several reasons: firstly, the diameter of the wire has not been measured precisely; secondly, the two un-etched ends have a greater diameter and they increase the inertia of the wire. The model of the single wire is not good and we would need a model that takes into account also these massive ends. Anyway their effect is to lower the frequency, which means that the actual tension of the wire is greater than the one obtained with the formula written above. Since the goal of the experiment is just to make sure that even at 77 K we have a residual tension, we can be satisfied with this room temperature result.

### 4.3 Liquid Nitrogen Measurement

The copper housing and the NbTi wires have two different thermal expansion coefficients. In particular, as it can be seen in the figure 16, the thermal contraction of the NbTi is lower and hence the tension of the wires will decrease. To calculate the tension at a certain temperature, we can consider the system as two springs

in parallel. Then, knowing the Young's module of the NbTi, the initial tension and the area of the wires, it is possible to find the cold tension:

$$T_c = T_w - E\,A\left(\frac{\Delta L_{Cu}}{L} - \frac{\Delta L_{NbTi}}{L}\right)$$

Where the Young module, E is $7*10^{10}\frac{N}{m^2}$, the area is $A = 7,55 *10^{-10}m^2$, $\frac{\Delta L_{Cu}}{L} = 0,003$ and $\frac{\Delta L_{NbTi}}{L} = 0,0014$. With a warm temperature of 30.63 g (for the wire 1), we obtain a cold tension of 22.01 g.
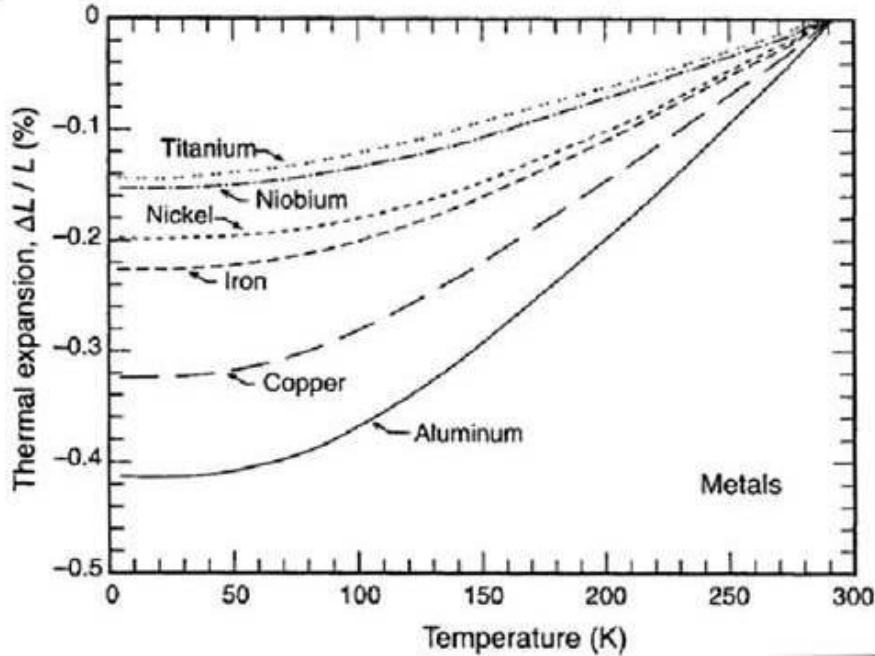


*Figure 16: Thermal expansion for a series of metals. Titanium and Niobium are very close, hence for the NbTi alloy an average value as been used.*

In order to experimentally verify this result, I have placed the coaxial cable in a chamber in liquid nitrogen. I have also put two temperature sensors, one on the top and one on the bottom, to verify that the temperature was close enough to 77 K. The temperature was measured with two sensors: in particular I have measured their resistance (keeping in mind the internal resistance of the voltmeter) and converted it to temperature with a table given by the manufacturer. Taking into account an offset calculated at room temperature, I have found that the final temperature at the bottom was around 75 K and at the top 80 K. Clearly, the temperature at the bottom must be around 77 K and the mismatch is due to the offset. We can be satisfied also with the temperature at the top, since an average temperature lower than 80K is enough for our purposes.

Firstly, I have measured both the resistance and the resonance frequency for the wire 1. In this way I have been able to make some considerations on the parameters, as the diameter of the wire, used in the calculations. In fact, I have found a mismatch of 20 Ω between the experimental resistance and the theoretical value, calculated considering the structure of the wires: indeed, since we have the two un-etched ends, we can treat it as a series of three parts: the first un-etched end, which in a parallel between the NbTi and the Cu, the central part, which is only NbTi, and the last end, which is again a parallel between Cu and NbTi. One way to solve this problem is to suppose that the diameter of the NbTi is actually 32.5 μm instead of 31 μm, hence 5% greater. This hypothesis gives a better agreement between the measurements and the theoretical calculation, as it can be seen in figure 17.
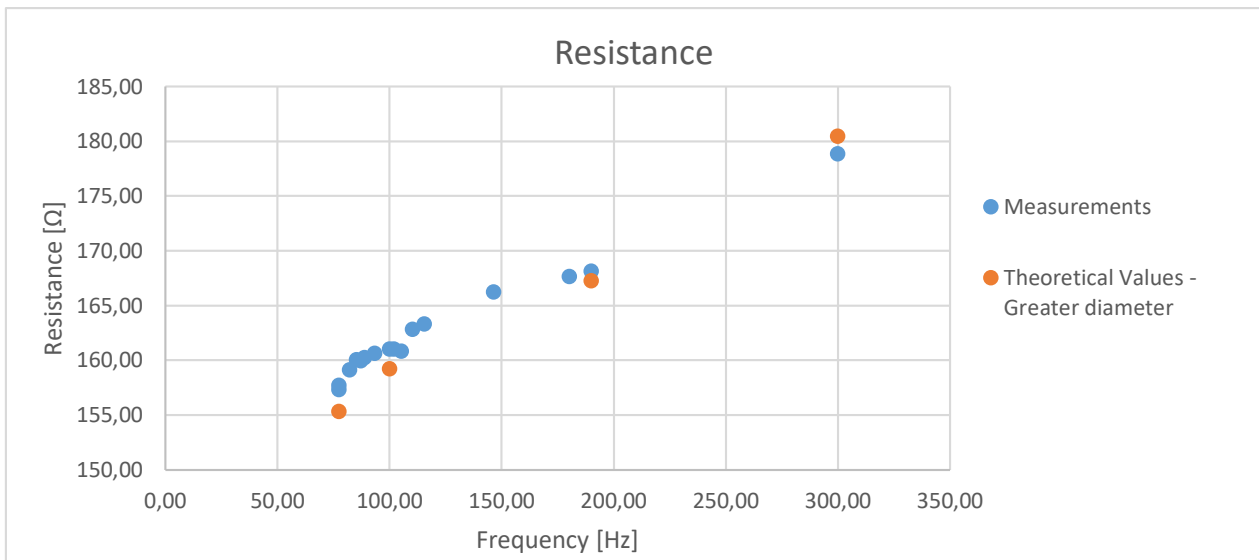
*Figure 17: comparison between the experimental data (in blue) and the theoretical values (in orange), obtained considering the wire as a series of three parts, composed by two parallel between Cu and NbTi, in series with a part of NbTi.*

Moreover, with this new value for the diameter, the warm tension is around 34 g, closer to the construction value of 40 g.

The measurement of the resonance frequency is more complicated at 77 K, since in order to reach this temperatures, it is also necessary to lower the pressure, down to $10^{-6}$ torr. At room temperature, the pressure can be kept at the level of the atmosphere, so the oscillations are damped by the air. In high vacuum, on the contrary, the oscillations are not damped and are greater, such that it is possible that the wire touches the copper housing, compromising the measurement of the resonance.
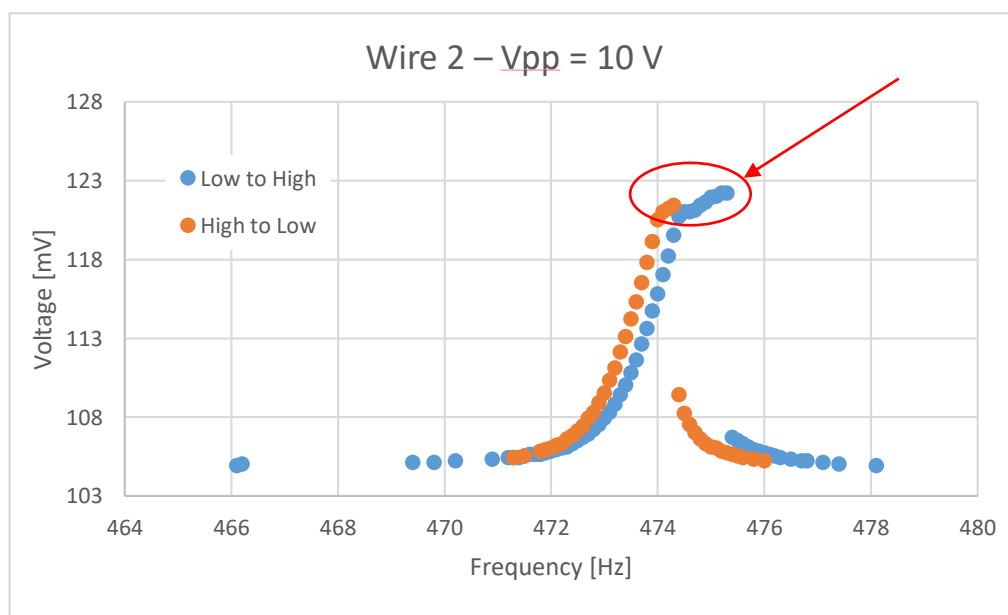


*Figure 18: measurement of the resonance peak in soft vacuum (around 1 torr). In the red circle, the wire is touching the housing. The values of the voltage are different if the frequencies are swept from high to low frequencies or viceversa. The peak seems to be asymmetric, due to the touching. The peak-to-peak voltage is 10 V. Lowering to 5 V, the wire doesn't touch the housing anymore and the peak is symmetric with a resonance frequency of 474 Hz.*

In soft vacuum, around 1 torr, the damping caused by air is already low and the oscillations are greater than the oscillations at atmospheric pressure. For this reason, the transversal speed of the wire oscillating is greater and the EMF induced is larger. As it can be seen in figure 18, the normalized peak high is four times the one we have in the measurements at atmospheric pressure. Since the wire is touching the housing, there are other two effects: the peak becomes asymmetric and there is a hysteresis. Indeed, the results obtained sweeping the frequency from high to low frequency are different from the results obtained in the opposite direction. In particular, going from low to high frequencies, when we hit the resonance and the wire touches the housing, the voltage across the wire keeps on increasing until at a certain point (that depends on the rate of the sweeping) the voltage falls back at its normal values. On the contrary, going from high to low frequencies, this hysteresis is not present and, once reached the resonance, the voltage across the wire abruptly gets higher and then decay as the frequency leaves the resonance frequency. The measurements in figure 18 were performed with a peak-to-peak voltage of 10 V, in order to show this effects. With a measurement with 5 V, the wire does not touch the housing and it is possible to recover a symmetric peak around 474 Hz. Hence, even if the wire is touching the housing, it is still possible to find the correct resonance frequency if the measurements are performed sweeping the frequencies from high to low values, in order to avoid the hysteresis.

At lower pressure ($10^{-6}$ torr), I have found that even with very small peak-to-peak voltages (i.e. 0.5 V), the wire touches the housing. For this reason, all the plots of the data taken at 77 K will have an asymmetric peak (figure 19).
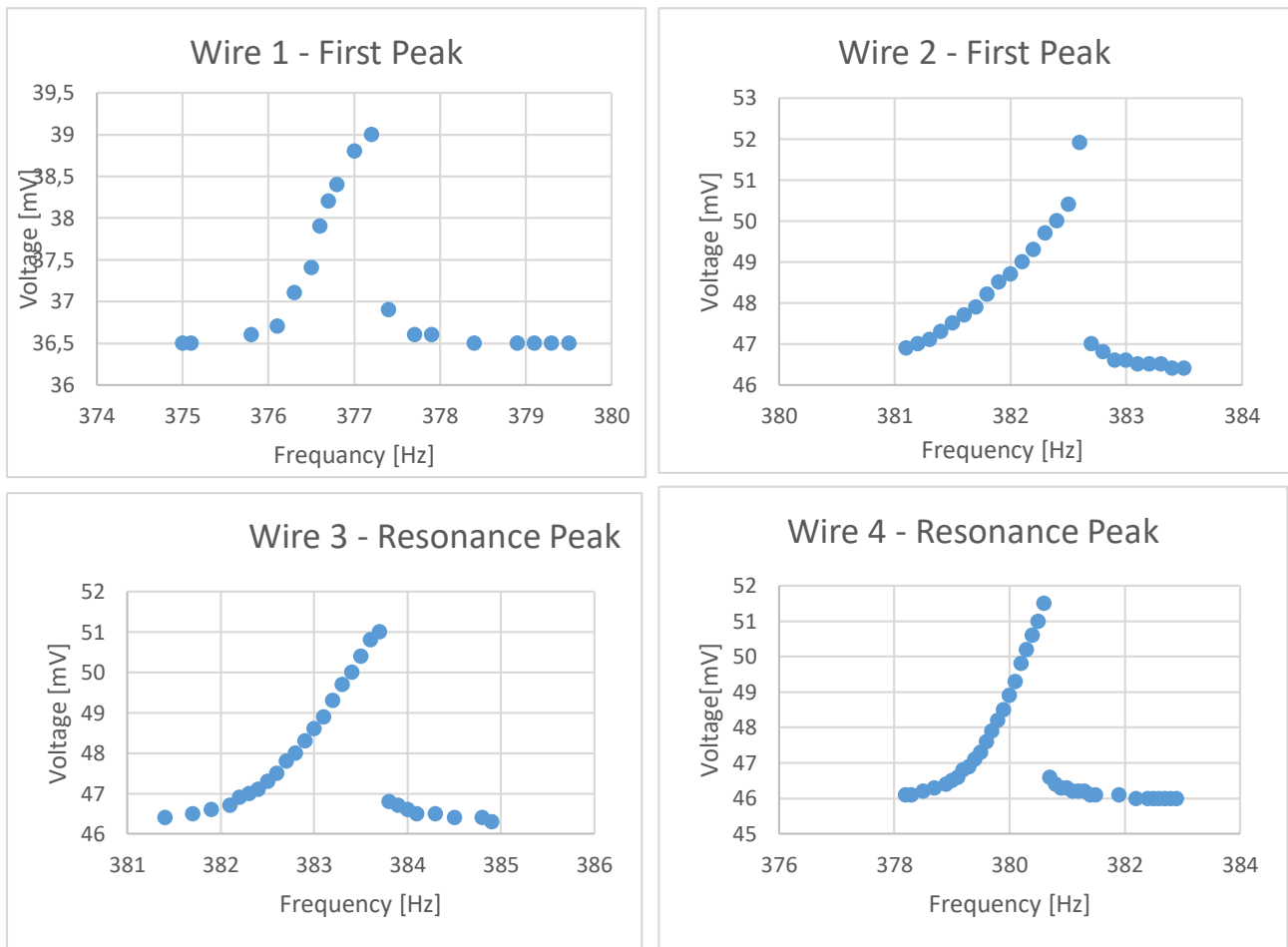


Figure 19: Resonance peaks for the 4 wires. The wire 1 has been measured with a $V_{pp}$ of 4 V, the other three with a $V_{pp}$ of 5 V, with a high to low sweeping. The resonance peaks are higher and asymmetric, due to the low pressure.

The resonance frequency at 77 K are all around 380 Hz, as it can be seen in table 4. In the same table there are also the values of the tension calculated with the formula employed also at room temperature. The average tension is around 20 g, in good agreement with the 22 g predicted theoretically.

|  | Wire 1 | Wire 2 | Wire 3 | Wire 4 |
|---|---|---|---|---|
| Resonance Frequency [Hz] | 377.2 | 382.6 | 383.7 | 380.6 |
| Tension [g] | 19.64 | 20.21 | 20.32 | 20.00 |

Table 4: Values of resonance frequency and tension for the 4 wires

The behavior of the tension and the frequency with temperature can be seen in figure 20, where the experimental data measured for the wire 1 have been plotted. Also, the 300 K and 77 K values for the other 3 wires have been added.
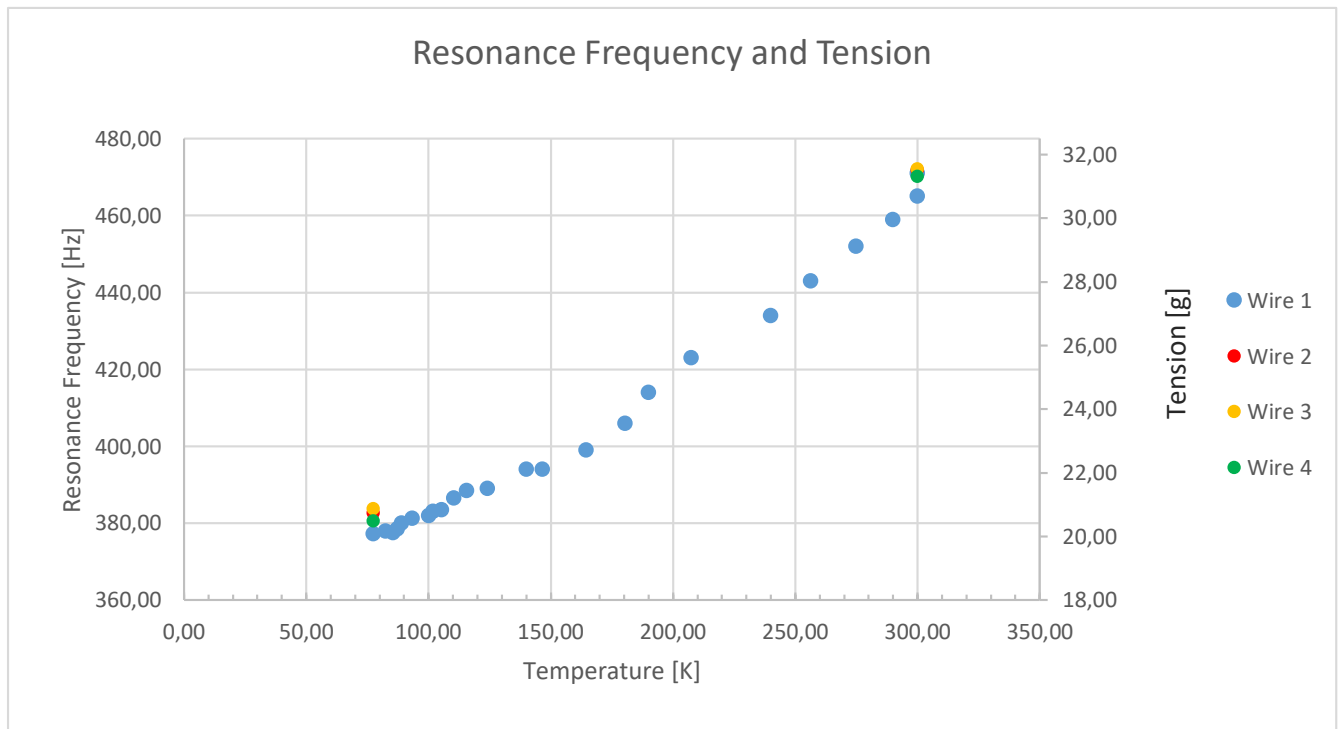


Figure 20: Tension and resonance frequency for each wire.

### 4.4 Conclusions

The measurements show that an initial tension of 40 g is enough to guarantee a minimum residual tension even at very low temperature. All the four wires that are present in the coaxial cable have similar values for the resonance frequency and hence for the tension. The measurement of the resistance, moreover, has shown that the value of the diameter could be slightly different from the one given by the manufacturer. Finally, it is important not to underestimate the importance of the low damping in high vacuum: in fact, a small mechanical vibration could induce an oscillation in the wires of the coaxial cable, causing a short cut with the housing and causing a high noise in the output signal. Anyway, the frequency of the normal mode of oscillation should be high enough to prevent this. In any case, the tension of the wire could be slightly increased (up to 60 g for example) to ensure this, without causing other problems or exceeding the elastic limit for the wires.

# 5  Bibliography

- Tang, A., Horton-Smith, G., Kudryavtsev, V.A. & Tonazzo, A., 2006. Muon simulations for Super-Kamiokande, KamLAND, and CHOOZ, *Phys. Rev. D,* **74,** 053007, doi:10.1103/PhysRevD.74.053007

- Lesparre, N., Gibert, D., Marteau, J., Declais, Y., Carbone, D., Galichet, E., 2010. Geophysical muon imaging: feasibility and limits, *Geophys. J. Int. ,* **183,** 1348-1361

- Bugaev, E. V., Misaki, A., Naumov, V.A., Sinegovskaya, T. S., Sinegovsky, S. I., Takahashi, N., 2000. Atmospheric Muon Flux at Sea Level, Underground and Underwater, arXiv:hep-ph/9803488v3 2 Jan 2000

- http://physics.nist.gov/PhysRefData/XrayMassCoef/tab1.html

- R. M. Sternheimer *et al*, Atomic Data & Nuclear Data Tables 30 (261), 1984

- Dunthil, P., Material Properties at Low Temperature

- Ekin, J. W., 2006, Experimental Techniques for Low-Temperature Measurements, Oxford University Press